nature structural & molecular biology

Modulation of protein properties in living cells using nanobodies

Axel Kirchhofer[1–3], Jonas Helma[2,4], Katrin Schmidthals[2,4], Carina Frauer[2,4], Sheng Cui[1–3], Annette Karcher[1–3], Mireille Pellis[5,6], Serge Muyldermans[5,6], Corella S Casas-Delucchi[7], M Cristina Cardoso[7], Heinrich Leonhardt[2,4,8], Karl-Peter Hopfner[1–3] & Ulrich Rothbauer[2,4,8,9]

Protein conformation is critically linked to function and often controlled by interactions with regulatory factors. Here we report the selection of camelid-derived single-domain antibodies (nanobodies) that modulate the conformation and spectral properties of the green fluorescent protein (GFP). One nanobody could reversibly reduce GFP fluorescence by a factor of 5, whereas its displacement by a second nanobody caused an increase by a factor of 10. Structural analysis of GFP–nanobody complexes revealed that the two nanobodies induce subtle opposing changes in the chromophore environment, leading to altered absorption properties. Unlike conventional antibodies, the small, stable nanobodies are functional in living cells. Nanobody-induced changes were detected by ratio imaging and used to monitor protein expression and subcellular localization as well as translocation events such as the tamoxifen-induced nuclear localization of estrogen receptor. This work demonstrates that protein conformations can be manipulated and studied with nanobodies in living cells.

Green fluorescent protein (GFP) is a barrel-shaped protein with a central *p*-hydroxybenzylidene-imidazolidone chromophore. The formation of the chromophore results from an oxidative backbone cyclization involving residues Ser65, Tyr66 and Gly67 (refs. 1–3). The original wild-type GFP (wtGFP) is characterized by a dual-peak excitation spectrum with a major absorption maximum at 395 nm and a minor one at 477 nm. Excitation at either wavelength results in the emission of green fluorescence at ~507 nm. This dual absorption of GFP stems from the existence of two interconvertible alternative states of the chromophore. The neutral phenol state of the chromophore absorbs at 395 nm, whereas the deprotonated phenolate anion absorbs at 477 nm[4]. During the past decade, the fluorescence properties of GFP have been successfully modified by mutagenesis[5–7]. For example, the most widely used mutant, enhanced GFP (eGFP), features increased brightness, improved photostability and a single excitation peak at 488–490 nm[5]. Additional types of bioimaging applications became possible with the photoactivatable (paGFP) variant[8]. Recently, new permuted GFP derivates were described as molecular sensors to monitor the presence of calcium, which induces structural rearrangements that block solvent access to the chromophore[9,10].

Here we investigated whether spectral properties of fluorescent proteins can be modulated with antibody derivatives. For this purpose, we tested so-called 'nanobodies', which are small, antigen-binding, single-domain polypeptides derived from the variable heavy chain (VHH) of the heavy chain–only antibodies of camelids[11]. Nanobodies are potent alternatives to conventional antibodies, with enhanced stability and reduced size but similar antigen-binding characteristics[12]. Applications described thus far include targeting and tracing of antigens in live cells and targeted modulation of enzymes as well as their usage as immobilized nanotraps to precipitate protein complexes *in vivo* and *in vitro*[13–17].

RESULTS

Generation of GFP-binding nanobodies

To isolate and characterize GFP-binding nanobodies, we generated a phagemid library by cloning the VHH repertoire from the heavy-chain antibodies of GFP-immunized camelids. Next, we displayed the VHH repertoire on phage particles and selected individual GFP-specific binders after panning followed by a solid-phase ELISA screening. Seven unique GFP-specific binders were determined by DNA sequence analysis of the clones. We termed the resulting proteins GFP-binding proteins (GBPs) 1–7. The GBPs were cloned with a C-terminal hexahistidine (His_6) tag, expressed in *Escherichia coli* and purified by immobilized metal affinity chromatography (IMAC). All GBPs coelute with wtGFP in an apparent 1:1 complex in gel filtration chromatography, verifying their stable binding to wtGFP (data not shown).

Nanobodies affecting GFP fluorescence intensity

To screen for nanobodies that alter GFP fluorescence properties, we added increasing amounts of GBP1–7 to wtGFP and measured the fluorescence intensity. We identified two nanobodies, GBP1 and

[1]Gene Center at the Department of Chemistry and Biochemistry, Ludwig-Maximilians University Munich, Munich, Germany. [2]Center for Integrated Protein Science, Munich, Germany. [3]Munich Center for Advanced Photonics, Munich, Germany. [4]Biocenter at the Department of Biology II, Ludwig-Maximilians University Munich, Planegg-Martinsried, Germany. [5]Department of Molecular and Cellular Interactions and [6]Laboratory of Cellular and Molecular Immunology, Vrije Universiteit Brussel, Brussels, Belgium. [7]Department of Biology, Technische Universität Darmstadt, Darmstadt, Germany. [8]Center for NanoScience, Ludwig-Maximilians University Munich, Munich, Germany. [9]ChromoTek GmbH, Planegg-Martinsried, Germany. Correspondence should be addressed to H.L. (H.Leonhardt@lmu.de), K.-P.H. (Hopfner@lmb.uni-muenchen.de) or U.R. (U.Rothbauer@chromotek.com).

Received 4 June; accepted 21 October; published online 13 December 2009; doi:10.1038/nsmb.1727

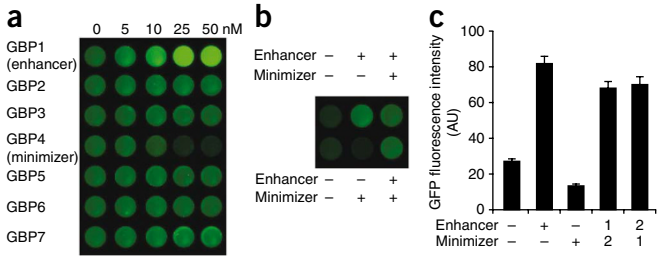

Figure 1 Identification of nanobodies modulating the fluorescence of GFP. (**a**) Fluorescence *in vitro* binding assay. Titration of seven unique GFP binding proteins (GBP1–7) from 0–50 nM on 50 nM purified wtGFP. The fluorescence signal intensity of wtGFP was quantified using a laser scanner. (**b**) Minimizer can be displaced by Enhancer but not vice versa. Upper row, GFP was either mock incubated or incubated with equimolar amounts of Enhancer, or Enhancer was added followed immediately (5–15 s) by equimolar amounts of Minimizer. Lower row, same experimental setup as above but with Minimizer being added first. GFP emission was detected as described for **a**. (**c**) Quantification of GFP fluorescence as shown in **b**. The order of addition of Enhancer or Minimizer is indicated by numbers 1 and 2. Means and s.d. (error bars) of three independent experiments are shown.

GBP4, that had a pronounced effect on the fluorescence emission of wtGFP (**Fig. 1a** and **Supplementary Fig. 1a**). Whereas binding of GBP1 leads to a fourfold fluorescence enhancement, binding of GBP4 reduces the fluorescence by a factor of 5. Overall, there is a remarkable 20-fold difference in fluorescence intensity between the two GFP–nanobody complexes under the conditions used. According to their observed impact on GFP fluorescence, we termed GBP1 and GBP4 'Enhancer' and 'Minimizer', respectively. The augmented fluorescence of the GFP–Enhancer complex is comparable to the improved spectral properties of eGFP. This raised the question of whether Enhancer might be able to further increase the optimized fluorescence of eGFP. Indeed, binding of Enhancer to recombinantly purified eGFP resulted in an additional fluorescence increase of about 1.5-fold. In contrast, binding of Minimizer reduced the fluorescence intensity of eGFP by a factor of 8 (**Supplementary Fig. 1b**,**c**). A comparable fluorescence modulation was also observed after addition of Enhancer or Minimizer to soluble cell extract derived from human embryonic kidney (HEK) 293T cells expressing eGFP (**Supplementary Fig. 1c**). To investigate whether selected nanobodies recognize different epitopes, we performed sandwich-binding assays. Additive binding to already-constituted GFP–Enhancer complexes could be detected for GBP2, GBP5, GBP6 and GBP7 but not for Minimizer, suggesting that Enhancer and Minimizer compete for overlapping epitopes of GFP (**Supplementary Fig. 2a**).

Based on the opposite effects of Enhancer and Minimizer binding, we investigated the wtGFP fluorescence modulation in the presence of both nanobodies (**Fig. 1b**,**c**). Notably, after a primary addition of Enhancer, wtGFP fluorescence increases and is only slightly reduced by the consecutive addition of Minimizer (**Fig. 1c**). In contrast, when Minimizer is added first, the reduction of fluorescence can be completely reversed, and fluorescence further enhanced, by subsequent addition of Enhancer (**Fig. 1c**). Although the ability of Enhancer to displace Minimizer at equimolar concentrations suggests that Enhancer has a higher affinity for wtGFP, no substantial difference in binding constants (K_d) was detected (**Supplementary Fig. 2b** and **Supplementary Table 1**).

Structure of GFP–Enhancer and GFP–Minimizer complexes

To elucidate the molecular mechanism underlying the observed fluorescence modulation, we determined crystal structures of the GFP–Enhancer and GFP–Minimizer complexes to 2.15 and 1.6 Å resolution, respectively (**Table 1**). Both nanobodies recognize two different, slightly overlapping epitopes on the GFP surface (**Fig. 2a**,**b**). Thus, the observed competition for binding seems to result from a steric clash between the nanobodies. Enhancer binds wtGFP in a frontwise manner at an exposed loop region between GFP β-strands 6 and 7 as well as parts of β-strand 8, making specific contacts with all three complementarity-determining regions (CDR) of the nanobody (**Fig. 2a**). Previous structural studies of nanobodies have shown that CDR3 normally folds over the framework 2 region, which in the case of classical antibodies binds to the variable domain of the light chain (VL)[18]. In contrast, the extremely short CDR3 of Enhancer is stretched out, thereby making the framework 2 region accessible to solvent in the antigen-free form. Unexpectedly, the entire framework 2 area participates in GFP recognition, in contrast to the structure of classical antibodies where the framework 2 area would contact the VL domain. The majority of the specific contacts are formed between CDR3 and GFP, whereas CDR1 and 2 remain exposed to the solvent. Notably, the interaction between GFP and Enhancer is predominantly electrostatic, spanning an interface of 672 Å^2 (**Supplementary Table 2**). An additional nonpolar contact is mediated by Phe98^{Enhancer}, which binds a hydrophobic surface patch on GFP formed by Ala206^{GFP}, Leu221^{GFP} and Phe223^{GFP}.

In contrast, the Minimizer nanobody has its CDR3 folded over the framework 2 region and binds wtGFP in a sideways orientation, using its elongated CDR3 to target β-strands 6 and 7 of GFP (**Fig. 2c**). The interaction with GFP is quite remarkable, since the nanobody targets the rigid and flat surface rather than the more flexible and easily accessible loops at the top and the bottom of the β-can. In comparison to Enhancer, Minimizer occupies a smaller surface area (652 Å^2) on GFP and the overall number of contacts is smaller (**Supplementary Table 3**). This observation is in line with its ready displacement by Enhancer in the competition assay (**Fig. 1c**). However, it is difficult

Table 1 Data collection and refinement statistics

	SeMet–GFP–Enhancer	GFP–Minimizer
Data collection		
Space group	$P4_222$	$P2_12_12_1$
Cell dimensions		
a, *b*, *c* (Å)	160.5, 160.5, 78.8	50.8, 81.6, 94.5
	Peak	
Wavelength (Å)	0.9793	0.98137
Resolution (Å)	2.15	1.5
R_{sym}	4.6 (45.4)[a]	5.7 (39.1)
$I / \sigma I$	14.95 (2.25)	16.91 (2.84)
Completeness (%)	99.3 (98.9)	97.5 (86.3)
Redundancy	3.13[b]	3.85
Refinement		
Resolution (Å)	46.00-2.15	47.00-1.61
No. reflections	56,271	49,989
R_{work}/R_{free}	21.3/25.5	16.1/19.4
No. atoms		
Protein	5,385	2,818
Water	407	685
B-factors		
Protein (Å^2)	46.5	13.7
Water (Å^2)	48.4	30.1
R.m.s. deviations		
Bond lengths (Å)	0.008	0.005
Bond angles (°)	1.14	1.04

[a]The structures of SeMet–GFP–Enhancer and of native GFP–Minimizer were determined with one crystal each. Values in parentheses are for highest-resolution shell. [b]For SeMet–GFP–Enhancer the anomalous redundancy is calculated.

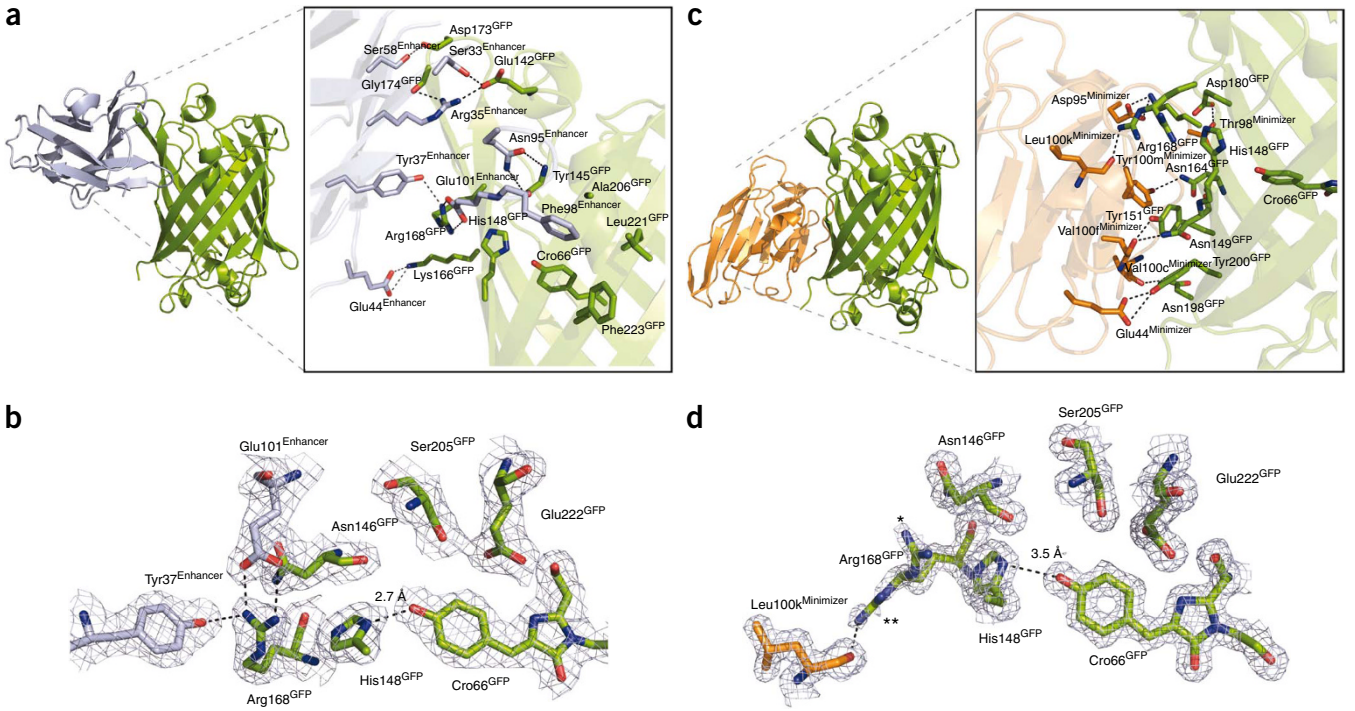

Figure 2 Structures of the GFP–nanobody complexes. (**a**–**d**) Enhancer (**a**; light blue ribbon model) and Minimizer (**c**) (orange ribbon model) recognize two different nonlinear epitopes on the surface of the GFP β-can (green ribbon model). The insets in **a** and **c** show details of the binding sites with selected residues and the GFP chromophore (Cro66^{GFP}) highlighted as sticks. The chromophore environments for the GFP–Enhancer (**b**) and GFP–Minimizer complexes (**d**), respectively, are superimposed with $2F_o - F_c$ density maps (contoured at 1.0σ). Two alternative conformations of R168^{GFP} are marked with * and **. Nanobody residues numbered as previously described[19]; in Minimizer, the 15 residues corresponding to position 100 are labeled a-o.

to quantitatively judge binding strengths from the structurally observed number of contacts or buried surface areas.

Induced rearrangements in the GFP chromophore environment

In general, association of the nanobodies has no substantial global influence on the overall fold of GFP. Unbound GFP (PDB 1EMB (ref. 4)) has r.m.s. deviations of 0.391 Å (Cα atoms) and 0.359 Å (Cα atoms) from GFP in complex with Enhancer and Minimizer, respectively. From previous structural studies of GFP, however, it is well established that slight perturbations in the chromophore environment can have vast effects on its fluorescence properties[4]. Indeed, a comparison of the GFP nanobody structures with previously published GFP structures reveals that the GFP–Enhancer complex harbors the deprotonated, negatively charged state of the GFP chromophore, which has been described for the mutant GFP^{S65T} (ref. 4) (**Fig. 2d**). Binding of Enhancer induces slight structural shifts in the loop region from Glu142^{GFP} to His148^{GFP} and fixes Arg168^{GFP} in close proximity to His148^{GFP}. The conformation of the Arg168^{GFP} side chain is stabilized by direct contacts with Enhancer residues Tyr37^{Enhancer} and Glu101^{Enhancer} (nanobody residues numbered as previously described[19]). These structural rearrangements bring the proton acceptor His148^{GFP} into very close proximity to the hydroxyl group of the GFP chromophore (distance 2.7 Å, compared to 2.8 Å for GFP^{S65T} and 3.4 Å for wtGFP). Thus, it is likely that binding of Enhancer facilitates improved proton extraction from the chromophore hydroxyl by His148^{GFP}, thereby stabilizing the phenolate anion of the chromophore and enhancing the fluorescence intensity. In contrast, the chromophore environment of the GFP–Minimizer complex is considerably different and shows similarities to the situation present in wtGFP[4]. Notably, Arg168^{GFP} is rather flexible in comparison to the Enhancer complex: we could trace two alternative conformations of its guanidine group in the electron density. In one of the conformations, Arg168^{GFP} is tilted away from His148^{GFP} and instead makes specific contacts with the backbone carbonyl of Leu100k^{Minimizer} (following the Kabat numbering[19]; the 15 residues corresponding to this position in Minimizer were labeled a-o). This nanobody-induced conformational change reduces the electrostatic forces exerted on His148^{GFP}, which is pulled back from the hydroxyl group of the chromophore and positioned with 3.5-Å distance (wtGFP: 3.4 Å) (**Fig. 2b**), too far to efficiently stabilize the phenolate anion. Instead, binding of Minimizer likely stabilizes an arrangement of the chromophore's surrounding environment that favors the neutral phenol state of the chromophore. In support of this model, binding of Enhancer to eGFP—where the phenolate anion state is stabilized by an engineered mutation—leads to an increase by a factor of 1.5 compared to a factor of 5 for wtGFP for wtGFP, whereas the fluorescence intensity is suppressed by Minimizer binding by a factor of 8 for eGFP compared to a factor of 4 for wtGFP. In summary, these two nanobodies appear to recognize and thermodynamically stabilize two conformational states of GFP, which affect the protonation state and thereby the spectral properties of the chromophore.

Enhancer and Minimizer modulate spectral properties of GFP

To directly test our structure-derived hypothesis that the interactions of the two nanobodies stabilize either the neutral or the ionized state of the chromophore, we analyzed the fluorescence absorption spectra of GFP in complex with either Enhancer or Minimizer (**Fig. 3a**,**b**). In support of our model, Enhancer increased absorption at 475 nm while reducing it at 395 nm for both wtGFP and eGFP. Minimizer modulated the absorption in exactly the opposite manner, reducing absorption at 475 nm and increasing it at 395 nm. We did not observe substantial changes in fluorescence lifetime upon Enhancer or Minimizer binding (**Supplementary Table 4**).

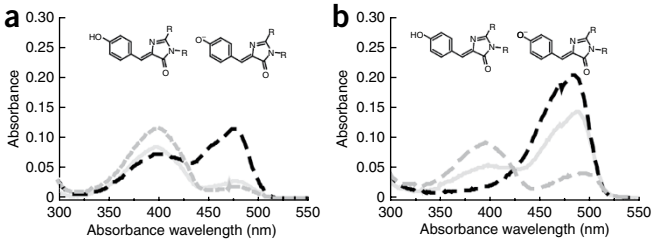

Figure 3 Nanobody-induced modulation of GFP spectral properties. Absorption spectra of the unbound (gray, solid line), Minimizer-bound (gray, dashed line) or Enhancer-bound (black, dashed line) wtGFP (**a**) or eGFP (**b**). The absorption at 395 nm corresponds to the protonated chromophore and absorption at 475 nm to the anionic chromophore (see chemical structures above).

Therefore, the fluorescence modulation upon nanobody binding is likely due to a change in the absorption efficiency at different wavelengths, which correlates with the magnitude of fluorescence emission and can be attributed to the protonation state of the chromophore.

Modulation of spectral properties of GFP in living cells

We next tested whether the nanobody-induced fluorescence modulation observed *in vitro* also occurs in living cells. To this end, we transfected human embryonic kidney (HEK) 293T cells with expression vectors encoding wtGFP or eGFP in combination with constructs encoding Enhancer, Minimizer or a control nanobody fused to monomeric red fluorescent protein (mRFP). Two days after transfection, we performed combined excitation and emission scans of GFP fluorescence intensities in living cells (**Fig. 4a**,**b** and **Supplementary Figs. 3** and **4**). Indeed, both nanobodies induced similar spectral changes in wtGFP and eGFP fluorescence, which demonstrates that Enhancer as well as Minimizer can effectively modulate GFP fluorescence in living cells. To obtain a concentration-independent measure of Enhancer or Minimizer binding and test whether subcellular differences can be detected, we determined the induced shift of GFP absorption maxima from 405 nm to 488 nm by ratio imaging. We tethered the Enhancer to the nuclear lamina by transfecting HeLa cells with an expression construct coding for an Enhancer–lamin B1 fusion. This fusion protein is incorporated into the nuclear lamina, generating an intranuclear binding site for GFP. After coexpressing wtGFP in excess, we acquired images with excitations at 405 nm and at 488 nm to detect relative differences in GFP fluorescence intensities at the nuclear lamina due to binding to locally immobilized Enhancer–lamin B1 fusion protein. Although GFP was bound and enriched at the nuclear lamina, this structure was barely detectable after excitation at 405 nm. However, excitation at 488 nm led to an increased signal at the nuclear lamina (**Fig. 4c**). The presence of Enhancer at this distinct subcellular structure could be visualized by calculating the ratio between pixel

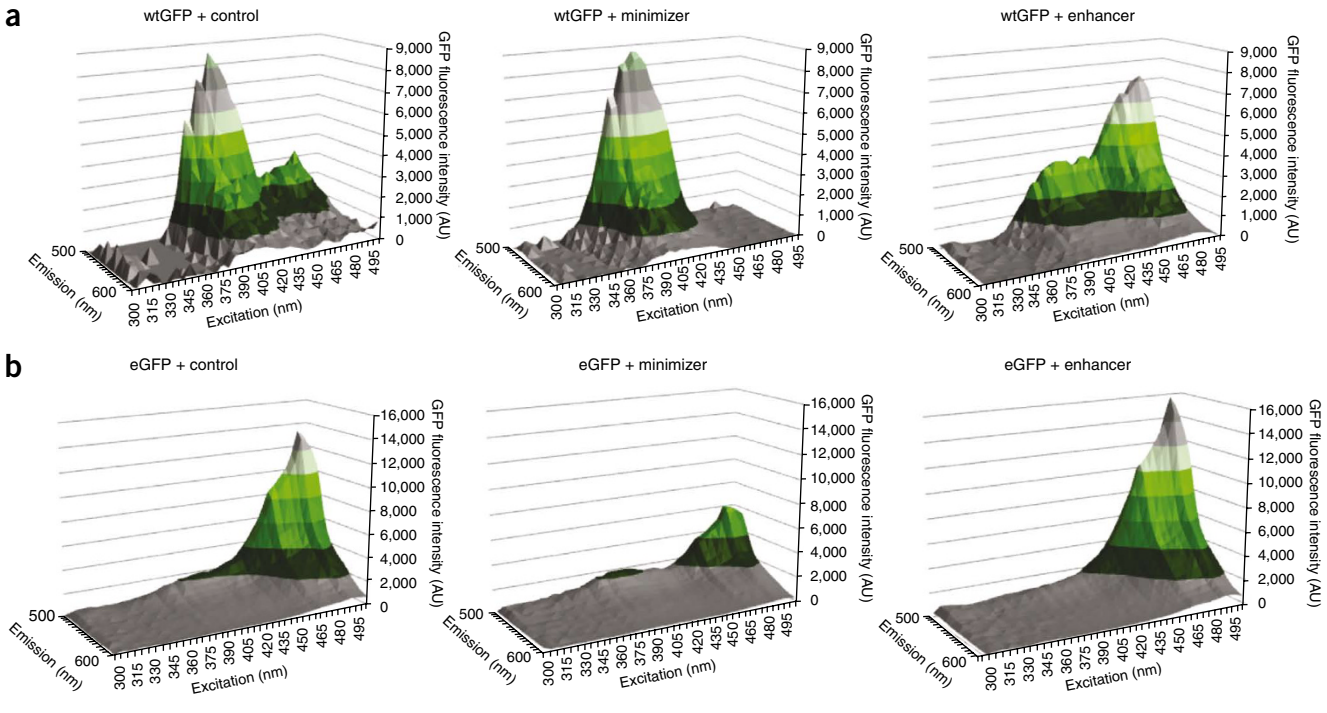

Figure 4 Nanobodies modulate GFP fluorescence in living cells. (**a**,**b**) Binding of Minimizer and Enhancer shifts excitation and emission spectra of both wtGFP (**a**) and eGFP (**b**) in living cells. (**c**) Ratio imaging. Shown are cells expressing wtGFP, which is dispersedly distributed. The topmost cell coexpresses Enhancer fused to lamin B1 (GBP1–lamin B1). Whereas only a weak signal at the nuclear lamina is detectable with excitation at 405 nm, the relative and absolute signal increased with excitation at 488 nm. Bound and unbound GFP can be distinguished independently by matrix algebra calculating the ratio between the signal intensities obtained with excitation at 488 nm and 405 nm for every pixel. The 488 nm/405 nm ratios are displayed in a false color gradient from blue (unbound) to yellow (bound). Scale bar is 10 μm.

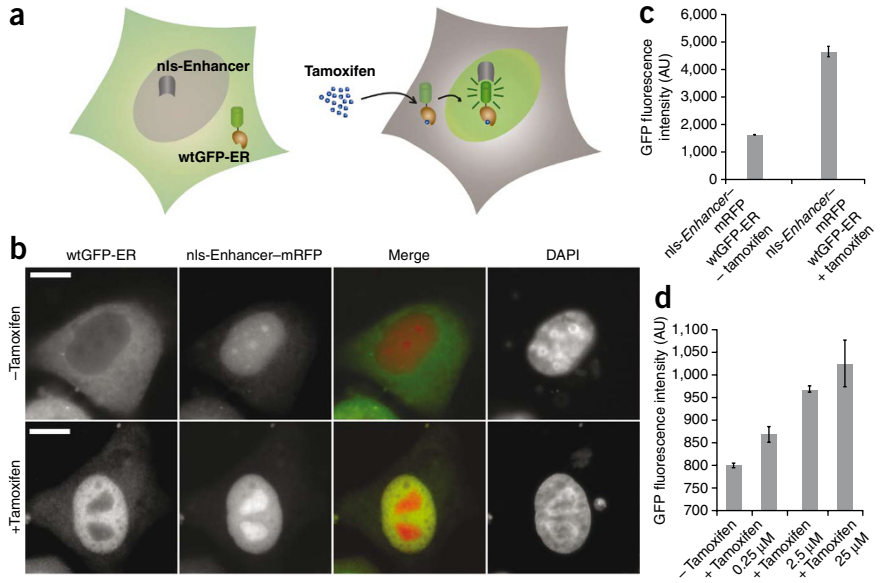

Figure 5 Nucleocytoplasmic translocation detected by nanobody-mediated fluorescence enhancement. (**a**) Schematic outline of the translocation assay: GFP-ER$_{286–595}$ and nls-Enhancer are present in separate compartments, the cytoplasm and the nucleus. Addition of tamoxifen induces translocation of GFP-ER$_{286–595}$ to the nucleus, where it binds to nls-Enhancer, leading to an increase of the fluorescence intensity. (**b**) Representative cells were analyzed by fluorescence microscopy (scale bar: 10 µM). Untreated cells (–Tamoxifen, upper row) show an almost exclusive distribution of GFP-ER$_{286–595}$ to the cytoplasm, whereas the nls-Enhancer is localized in the nucleus. After addition of tamoxifen (+Tamoxifen, lower row) GFP-ER$_{286–595}$ colocalizes with nls-Enhancer in the nucleus. (**c**,**d**) Nucleocytoplasmic translocation was measured in a plate format in living cells by detection of GFP fluorescence intensity. (**c**) After translocation of GFP-ER$_{286–595}$ into the nucleus upon addition of tamoxifen, binding of nls-Enhancer leads to a three-fold increase in fluorescence intensity. (**d**) Detection of the dose-dependent translocation efficiency after addition of increasing concentrations of tamoxifen (as indicated). Means and s.d. (error bars) of three independent experiments are shown.

intensities obtained at 405 nm and at 488 nm and displaying the ratio images in false color, thereby distinguishing bound and unbound GFP (**Fig. 4c**). This example illustrates how fluorescence-modulating nanobodies can provide novel optical readouts.

Tracking of subcellular translocation processes

Finally, we tested whether the fluorescence-enhancement effect induced by binding of GFP to Enhancer localized in a defined subcellular compartment could be used to track subcellular translocation events in a high-throughput approach. As an example, we used the inducible translocation of the human estrogen receptor. Hormone binding leads to a conformational change in the receptor that results in its dissociation from chaperone proteins and ultimately in its binding as a homodimer to cognate sites in steroid-responsive genes[20]. This subcellular trafficking event can be induced by the synthetic steroid hormone tamoxifen and followed with a GFP-labeled receptor and high-resolution fluorescence microscopy[21]. Because this procedure is based on single-cell imaging, it is poorly suited for high-throughput analyses. We generated a mammalian (HeLa-Kyoto) cell line that stably expresses nuclear-localized Enhancer fused to mRFP (nls-Enhancer). As described previously, GFP nanobodies can specifically recognize and bind to their respective epitopes in various subcellular compartments in living cells[16]. The cellular expression of the nanobodies has no obvious cytotoxic effect, as no differences in cell-based proliferation analysis of the nls-Enhancer–encoding cell line compared to the parental cell line could be detected (data not shown). We used the newly constructed cell line to transiently coexpress the steroid-binding domain of the human estrogen receptor (ER$_{286–595}$) fused to wtGFP (GFP-ER$_{286–595}$). According to our assay, translocation of this construct from the cytoplasm to the nucleus should be detectable by an increase of the GFP fluorescence intensity upon binding of GFP to the nls-Enhancer in the nucleus (**Fig. 5a**). Using fluorescence microscopy, we confirmed that both GFP-ER$_{286–595}$ and nls-Enhancer are almost exclusively localized in their designated compartments. Upon addition of tamoxifen to the medium, GFP-ER$_{286–595}$ translocated from the cytoplasm into the nucleus (**Fig. 5b**). After entering the nucleus, GFP becomes accessible for binding to nls-Enhancer, which results in a three-fold increase in GFP fluorescence intensity (**Fig. 5c**). Notably, the translocation event can be followed in a statistically significant number of cells by scanning the fluorescence intensities of living cells in multiwell formats. The fluorescence enhancement is directly correlated with translocation efficiency. By quantifying the fluorescence intensities, we detected a clear dose dependence of translocation on addition of increasing amounts of tamoxifen (**Fig. 5d**). Because our assay is based on living cells, we were able to follow the dynamics of the translocation event over time. These data demonstrate that fluorescence-modulating nanobodies are potent tools for studying subcellular relocalization, a key process of signal transduction, in real time and in a quantitative manner.

DISCUSSION

Alternative protein conformations can be accurately analyzed with a variety of biophysical methods *in vitro* but are notoriously difficult to study *in vivo*. We therefore tested whether recombinantly expressed nanobodies could discriminate between alternative protein conformations in living cells. As a target we chose GFP, as it provides a direct optical readout. Out of several GFP-specific nanobodies, we identified two, Minimizer and Enhancer, that shift the absorption of GFP in opposite directions. The corresponding crystal structures clearly show the structural changes induced by these two nanobodies and explain the functional consequences on GFP fluorescence.

This ability to manipulate protein conformation in living cells enables a number of new applications. As a first example, we use the modulation of GFP fluorescence for new bioimaging applications. The expression and subcellular distribution of Minimizer and Enhancer can be detected by ratio imaging, allowing the distinction of bound and unbound GFP. This indirect optical readout can be used as reporter for gene expression, virus infection and translocation assays. The nanobody-mediated enhancement of GFP fluorescence should also improve the tracing of low- to high-abundance GFP fusion proteins in live cells as well as ultrahigh resolution microscopy. We have recently demonstrated that cellular structures can be imaged at subdiffraction resolution by three-dimensional structured illumination microscopy (3D-SIM)[22]. To obtain ultrahigh resolution, however,

this new microscopy technology requires hundreds of images and thus mostly relies on bright synthetic chromophores. The signals obtained with physiological levels of GFP-labeled proteins are barely sufficient, and in particular, *in vivo* application of structured illumination[23] would greatly benefit from any fluorescence enhancement by a coexpressed Enhancer nanobody.

Translocation events have a central role in signal transduction and are therefore a prime target for drug screenings. Presently, translocations are monitored either with reporter gene assays, which take at least a day, or by microscopy, which requires costly and technically demanding high-throughput image acquisition and analysis tools. Our nanobody-based assay can be performed with a simple plate reader and measures translocation as fluorescence enhancement after drug addition. We demonstrate the feasibility of this assay principle using the tamoxifen-induced nuclear translocation of the estrogen receptor. Aside from steroid hormone receptors, notch-type signaling in differentiation and cancer could also be directly monitored in cell-based drug screens.

This work outlines new experimental possibilities as it exemplifies applications of nanobodies ranging from affinity purification and crystallization of proteins to the manipulation of conformational states and protein function *in vitro* and in living cells. In particular, the detection and manipulation of alternative protein conformations in living cells enable novel types of studies in molecular and cellular biology. The functional relevance of alternative protein conformations is clearly illustrated by the prion protein. Here we outline and demonstrate an experimental strategy to address the role of alternative protein conformations in cellular systems. Our results show that nanobodies can be generated to recognize, induce and stabilize alternative protein conformations and thus enable studies of functional properties of specific protein conformations *in vitro* and *in vivo*.

METHODS

Methods and any associated references are available in the online version of the paper at http://www.nature.com/nsmb/.

Accession codes. Protein Data Bank: Coordinates and structure factors for the GFP-Enhancer and GFP-Minimizer complex were deposited with accession codes 3K1K and 3G9A, respectively.

Note: Supplementary information is available on the Nature Structural & Molecular Biology website.

ACKNOWLEDGMENTS

A. Kirchhofer acknowledges support from the Deutsche Forschungsgemeinschaft graduate school 1202. U.R., J.H. and K.S. were supported by the GO-Bio program (Bundesministeriums für Bildung und Forschung) and C.F. by the International Doctorate Program 'NanoBioTechnology' of the Elite Network of Bavaria. The authors thank J. Gregor for excellent technical assistance, K. Lammens for help with crystallographic data collection, R. Lewis for fluorescence lifetimes determination and K. Zolghadr and N. Hiller for helpful comments and suggestions. This work was supported by the Center for Integrated Protein Science (CIPSM), the Center for Nanoscience (CeNS), the Nanosystems Initiative Munich (NIM), the BioImaging Network (BIN) and grants from the Deutsche Forschungsgemeinschaft (DFG) to M.C.C., H.L. and K.-P.H. (SFB 684). A. Kirchhofer and K.-P.H. thank K. Römer and the Dr. Klaus Römer Foundation for financial support.

AUTHOR CONTRIBUTIONS

U.R., M.C.C. and H.L. conceived and initiated the original project; A. Kirchhofer crystallized the GFP–nanobody complexes, determined the crystal structures, carried out life-time measurements and wrote the manuscript; S.C. and A. Karcher assisted in crystallization and structure determination; K.-P.H. helped with interpreting structural and functional data as well as determining crystal structures, designing research and helped with writing the manuscript; M.P. and S.M. provided the nanobodies; J.H. performed *in vitro* nanobody binding studies; K.S. carried out nanobody and GFP purification; J.H., C.S.C.-D. and M.C.C. carried out the ratio imaging experiments; C.F. performed the *in vivo* studies and data analysis; H.L. wrote the manuscript; M.C.C., S.M., H.L. and K.-P.H. revised the manuscript and oversaw research. U.R. carried out nanobody purification, *in vitro* analysis, translocation assays and wrote the manuscript.

COMPETING INTERESTS STATEMENT

The authors declare competing financial interests: details accompany the full-text HTML version of the paper at http://www.nature.com/nsmb/.

Published online at http://www.nature.com/nsmb/.
Reprints and permissions information is available online at http://npg.nature.com/reprintsandpermissions/.

1. Chalfie, M., Tu, Y., Euskirchen, G., Ward, W.W. & Prasher, D.C. Green fluorescent protein as a marker for gene expression. *Science* **263**, 802–805 (1994).
2. Ormo, M. *et al.* Crystal structure of the *Aequorea victoria* green fluorescent protein. *Science* **273**, 1392–1395 (1996).
3. Yang, F., Moss, L.G. & Phillips, G.N. Jr. The molecular structure of green fluorescent protein. *Nat. Biotechnol.* **14**, 1246–1251 (1996).
4. Brejc, K. *et al.* Structural basis for dual excitation and photoisomerization of the *Aequorea victoria* green fluorescent protein. *Proc. Natl. Acad. Sci. USA* **94**, 2306–2311 (1997).
5. Heim, R. & Tsien, R.Y. Engineering green fluorescent protein for improved brightness, longer wavelengths and fluorescence resonance energy transfer. *Curr. Biol.* **6**, 178–182 (1996).
6. Tsien, R.Y. The green fluorescent protein. *Annu. Rev. Biochem.* **67**, 509–544 (1998).
7. Shimomura, O. Discovery of green fluorescent protein. *Methods Biochem. Anal.* **47**, 1–13 (2006).
8. Patterson, G.H. & Lippincott-Schwartz, J. A photoactivatable GFP for selective photolabeling of proteins and cells. *Science* **297**, 1873–1877 (2002).
9. Nakai, J., Ohkura, M. & Imoto, K. A high signal-to-noise Ca^{2+} probe composed of a single green fluorescent protein. *Nat. Biotechnol.* **19**, 137–141 (2001).
10. Akerboom, J. *et al.* Crystal structures of the GCaMP calcium sensor reveal the mechanism of fluorescence signal change and aid rational design. *J. Biol. Chem.* **284**, 6455–6464 (2009).
11. Hamers-Casterman, C. *et al.* Naturally occurring antibodies devoid of light chains. *Nature* **363**, 446–448 (1993).
12. Arbabi Ghahroudi, M., Desmyter, A., Wyns, L., Hamers, R. & Muyldermans, S. Selection and identification of single domain antibody fragments from camel heavy-chain antibodies. *FEBS Lett.* **414**, 521–526 (1997).
13. Muyldermans, S. Single domain camel antibodies: current status. *J. Biotechnol.* **74**, 277–302 (2001).
14. Jobling, S.A. *et al.* Immunomodulation of enzyme function in plants by single-domain antibody fragments. *Nat. Biotechnol.* **21**, 77–80 (2003).
15. Rothbauer, U. *et al.* A versatile nanotrap for biochemical and functional studies with fluorescent fusion proteins. *Mol. Cell. Proteomics* **7**, 282–289 (2008).
16. Rothbauer, U. *et al.* Targeting and tracing antigens in live cells with fluorescent nanobodies. *Nat. Methods* **3**, 887–889 (2006).
17. Chan, P.H. *et al.* Engineering a camelid antibody fragment that binds to the active site of human lysozyme and inhibits its conversion into amyloid fibrils. *Biochemistry* **47**, 11041–11054 (2008).
18. Desmyter, A. *et al.* Three camelid VHH domains in complex with porcine pancreatic alpha-amylase. Inhibition and versatility of binding topology. *J. Biol. Chem.* **277**, 23645–23650 (2002).
19. Kabat, E.A. & Wu, T.T. Identical V region amino acid sequences and segments of sequences in antibodies of different specificities. Relative contributions of VH and VL genes, minigenes, and complementarity-determining regions to binding of antibody-combining sites. *J. Immunol.* **147**, 1709–1719 (1991).
20. Tsai, M.J. & O'Malley, B.W. Molecular mechanisms of action of steroid/thyroid receptor superfamily members. *Annu. Rev. Biochem.* **63**, 451–486 (1994).
21. Htun, H., Holth, L.T., Walker, D., Davie, J.R. & Hager, G.L. Direct visualization of the human estrogen receptor alpha reveals a role for ligand in the nuclear distribution of the receptor. *Mol. Biol. Cell* **10**, 471–486 (1999).
22. Schermelleh, L. *et al.* Subdiffraction multicolor imaging of the nuclear periphery with 3D structured illumination microscopy. *Science* **320**, 1332–1336 (2008).
23. Kner, P., Chhun, B.B., Griffis, E.R., Winoto, L. & Gustafsson, M.G. Super-resolution video microscopy of live cells by structured illumination. *Nat. Methods* **6**, 339–342 (2009).

ONLINE METHODS

Protein production and purification. We carried out expression of nanobodies and GFP as described previously[15,24]. We produced selenomethionine (SeMet)-containing GFP in *E. coli* B834 (Rosetta (DE3)) grown in minimal medium containing 50 mg l^{-1} L-selenomethionine. For complex purification of wtGFP-Enhancer and wtGFP-Minimizer, we purified nanobodies by prebinding them via their C-terminal His_6 tag to a HiTrap-column (GE Healthcare Life Sciences). Subsequently, we isolated wtGFP from crude cell extracts by binding to the pre-charged column. After elution by increasing concentration of imidazole, we separated complexes from unbound protein by gel filtration chromatography using a Superdex 200 column (GE Healthcare).

Fluorescence spectroscopy. We performed fluorescence assays either by scanning a 96-well microplate (Nunc) on a Typhoon Trio (GE Healthcare; ex_{GFP}, 488 nm, em, 520 ± 20 nm) or by using a monochromator-based microplate reader (Infinite M1000, Tecan; ex_{wtGFP}, 395 nm, ex_{eGFP}, 488 nm, em, 507 ± 10 nm). We recorded fluorescence excitation spectra with a FluoroMax-P fluorimeter (HORIBA Jobin Yvon). Typically, a 0.5-μM protein in PBS was measured in a 1-ml quartz cuvette (ex./em. bandpass, 5 nm). Samples were excited at 395 nm and 475 nm, and excitation spectra were recorded in the range from 480–600 nm. We recorded fluorescence absorption spectra on a UV/Vis Spectrophotometer (Beckman Coulter). Absorptions of 0.5-μM GFP alone or 0.5-M GFP–Enhancer and –Minimizer complexes were detected with continuous excitation steps (1 nm) from 250 nm–700 nm.

Crystallization and data collection. We crystallized purified GFP–nanobody complexes by hanging-drop vapor diffusion by mixing 1 μl of protein solution at 10 mg ml^{-1} concentration with 1 μl of the reservoir solution (SeMet-GFP–Enhancer: 60% (v/v) 2-methyl-2,4-pentanediol (MPD), 100 mM sodium acetate pH 4.6, 10 mM $CaCl_2$; GFP–Minimizer: 100 mM 2-(*N*-morpholino)ethanesulfonic acid, pH 6.5, 30% (v/v) PEG8000, 15% (v/v) glycerol). Initial crystallographic data obtained from native GFP–Enhancer (data not shown) suffered from crystal twinning, and coordinate refinement after molecular replacement did not result in acceptable *R* values. Crystals of SeMet-GFP–Enhancer, originally grown to obtain experimental phases by anomalous dispersion, grew in a different space group without twinning. After flash freezing the crystals, we recorded single-wavelength diffraction data at the K absorption edge of selenium (λ = 0.9793 Å) at the X06SA beamline (Swiss Light Source) to 2.15 Å. GFP–Minimizer crystals were flash frozen in liquid nitrogen. Data collection was performed at the beamline ID29 (λ = 0.98137 Å) at the European Synchrotron Radiation Facility to a resolution of 1.6 Å.

Structure determination. We processed diffraction data of both complexes with XDS[25]. In the case of the GFP–Enhancer structure, we located three selenium sites per complex using autoSHARP (Global Phasing). Single-wavelength anomalous dispersion phasing and solvent flipping yielded an interpretable experimental electron density map. We built models for GFP and Enhancer with COOT[26] and refined them with PHENIX[27], using overall anisotropic *B*-factors and bulk solvent corrections, individual *B*-factor refinement, simulated annealing, and crystallographic and positional refinement. We determined the GFP–Minimizer structure by molecular replacement with PHASER using an individual GFP and a nanobody polypeptide chain from the previously determined GFP–Enhancer structure as independent search models. We manually altered and refined the replacement model with COOT using similar procedures as described for the GFP–Enhancer structure. All structure figures were prepared using the program PyMol (http://www.pymol.org/). Data collection and model statistics are summarized in **Table 1**.

Spectral analysis in living cells. We detected the overall fluorescence intensities of GFP and expression levels of mRFP fusions in HEK293T cells by fluorescence spectroscopy on a microplate reader (ex_{GFP}, 490 ± 5 nm, em_{GFP}, 511 ± 5 nm, ex_{mRFP}, 586 ± 5 nm, em_{mRFP}, 608 ± 5 nm). For spectral analysis we scanned the cells in intervals of 5 nm for excitation from 300–500 nm and for emission from 500–580 nm. To quantify and normalize the data to the relative expression levels of GFP, we lysed remaining cells and performed immunoblot analysis using a GFP antibody (Roche). Preparation of cells and calculations of GFP fluorescence values were performed as described in **Supplementary Methods**.

Ratio imaging. We recorded cells expressing wtGFP and the Enhancer fusion GBP1–lamin B1 with excitation laser lines at 405 nm or 488 nm (em_{GFP}, 527 ± 27 nm) using a spinning disk microscope (UltraVIEW VoX, Perkin Elmer). For noise reduction, a Gaussian filter (σ = 2) was applied to both images. To visualize altered spectral properties of GFP induced by Enhancer, binding signal intensities recorded with excitation at 488 nm were divided by the corresponding 405-nm intensities for each pixel. This 488/405 ratio was displayed in a false color gradient from blue (unbound) to yellow (bound). Image analysis operations were executed in Priithon, a Python-based image analysis and algorithm development platform. Preparation of cells was performed as described in **Supplementary Methods**.

Translocation assay. For the nucleocytoplasmic translocation assay, we transfected HeLaK cells stably expressing the Enhancer fused to mRFP comprising an N-terminal nuclear localization signal (nls-Enhancer) with an expression plasmid for a tamoxifen-responsive estrogen receptor domain fused to wtGFP (GFP-$ER_{286–595}$). Eighteen hours after transfection, about 50% of the cells were expressing GFP-$ER_{286–595}$ preferentially in the cytoplasm, whereas the nls-Enhancer–mRFP fusion protein was slightly enriched in the nucleoli as determined by fluorescence microscopy. We incubated ~1×10^7 cells with DMEM containing 0–25 μM tamoxifen for 30 min. We used an equal number of cells from the same transfection as an untreated control. We harvested the cells, washed them twice and resuspended them in 1 ml PBS. Roughly 3×10^6 cells were transferred to a 96-well plate (Greiner). We determined fluorescence intensities of GFP and mRFP by fluorescence spectroscopy (Tecan Infinite M1000 plate reader, ex_{GFP}, 490 ± 5 nm, em_{GFP}, 511 ± 5 nm, ex_{mRFP}, 586 ± 5 nm, em_{mRFP}, 608 ± 5 nm). We subtracted background fluorescence intensities from untransfected cells and normalized GFP fluorescence intensities against mRFP fluorescence intensity.

Materials. Purified Enhancer and Minimizer protein is commercially available from ChromoTek (Germany). Enhancer and Minimizer encoding vectors for intracellular studies can be requested from the Ludwig-Maximilians University, Munich.

24. Frauer, C. & Leonhardt, H. A versatile non-radioactive assay for DNA methyltransferase activity and DNA binding. *Nucleic Acids Res.* (2009).
25. Kabsch, W. Automatic processing of rotation diffraction data from crystals of initially unknown symmetry and cell constants. *J. Appl. Cryst.* **26**, 795–800 (1993).
26. Emsley, P. & Cowtan, K. Coot: model-building tools for molecular graphics. *Acta Crystallogr. D Biol. Crystallogr.* **60**, 2126–2132 (2004).
27. Adams, P.D. *et al.* PHENIX: building new software for automated crystallographic structure determination. *Acta Crystallogr. D Biol. Crystallogr.* **58**, 1948–1954 (2002).